ADVANCED FUNCTIONAL MATERIALS
www.afm-journal.de

4D Printing of Adaptable "Living" Materials Based on Alkoxyamine Chemistry

H.B. Duc Tran, Clara Vazquez-Martel, Samantha O. Catt, Yixuan Jia, Manuel Tsotsalas, Christoph A. Spiegel, and Eva Blasco**

4D printing has emerged as a powerful strategy capable of revolutionizing additive manufacturing by enabling objects to dynamically transform overtime on demand. Despite significant progress, the full potential remains unrealized, particularly in the utilization of dynamic covalent chemistry. This study introduces a new approach using a multifunctional cross-linker with alkoxyamine functionalities for 4D printing. Digital light processing (DLP) is employed for high-resolution printing of complex objects. Leveraging alkoxyamine bonds' dynamic and living characteristics, the printed structures can be further modified through nitroxide-mediated polymerization (NMP) using styrene and nitroxide exchange reactions (NER). The resulting "living" printed structures exhibit the unique ability to undergo both "growth" and "degrowth", dynamically adapting their size as well as the reduced Young's Modulus across a wide range (770 kPa–1.2 GPa). The chain extension by NMP and softening by NER are carefully characterized by IR and EPR spectroscopy. The presented approach opens avenues for the development of 4D printed structures with complex adaptive systems, showcasing enormous potential in a wide range of fields.

1. Introduction

The field of 3D printing, or additive manufacturing, has made remarkable strides in recent years, transforming the way we design, prototype, and manufacture objects across various applications.[1-6] However, the full potential of 3D printing is yet to be realized. An example of this emerging trend is the fabrication of 3D systems with adjustable properties, which is of particular interest in fields including biomedicine,[7-9] fluidic devices,[10–12] or soft robotics.[13-15] This strategy has been termed 4D printing, allowing the direct generation of smart geometries that are able to change shape, properties, or functionality over time in response to external stimuli. For this purpose, several strategies have been reported including the use of smart polymeric materials such as responsive hydrogels,[16-21] liquid crystal elastomers[22,23] and shape memory polymers[24-27] as well as the use of reversible deactivation radical polymerization methods, such as reversible addition-fragmentation chain-transfer polymerization (RAFT) polymerization.[28-31] Another promising method for introducing dynamic characteristics into 3D structures involves the incorporation of dynamic covalent chemistry. Dynamic covalent bonds have emerged as an exceptional type of chemistry, presenting distinctive advantages and opportunities.[32-35] They possess the remarkable ability to break and reform chemical bonds in contrast to static materials. This inherent dynamic behavior makes them highly adaptable and versatile, opening doors to novel material properties and applications.[36-43]

One intriguing avenue involves the incorporation of dynamic covalent bonds in the form of alkoxyamines. The alkoxyamine is an example of dynamic covalent bond, where stable nitroxide radicals serve in a dissociation-combination mechanism.[44] In polymeric networks, this chemistry allows for the incorporation of dynamic features, by tuning their degree of cross-linking and thus the mechanical properties by using nitroxide exchange reaction (NER) or chain extension via nitroxide-mediated polymerization (NMP).[45-50] Despite the great potential, alkoxyamine dynamic covalent chemistry has not yet been fully exploited in the field of additive manufacturing. Only very recently, the possibility of combining alkoxyamine chemistry with two-photon 3D laser printing was shown for the generation of adaptable 3D microstructures.[51,52] In particular, we reported a printable system based on nitroxide containing TEMPO-methacrylate and a soft diacrylate PEG cross-linker. By NMP chain extension using styrene as a monomer, we proved a large increase in volume as

H. D. Tran, C. Vazquez-Martel, S. O. Catt, C. A. Spiegel, E. Blasco
Institute for Molecular Systems Engineering and Advanced Materials
Heidelberg University
69120 Heidelberg, Germany
E-mail: christoph.spiegel@oci.uni-heidelberg.de;
eva.blasco@oci.uni-heidelberg.de

H. D. Tran, C. Vazquez-Martel, S. O. Catt, C. A. Spiegel, E. Blasco
Institute of Organic Chemistry
Heidelberg University
69120 Heidelberg, Germany

Y. Jia, M. Tsotsalas
Institute of Functional Interfaces
Karlsruhe Institute of Technology
76344 Eggenstein-Leopoldshafen, Germany

DOI: 10.1002/adfm.202315238

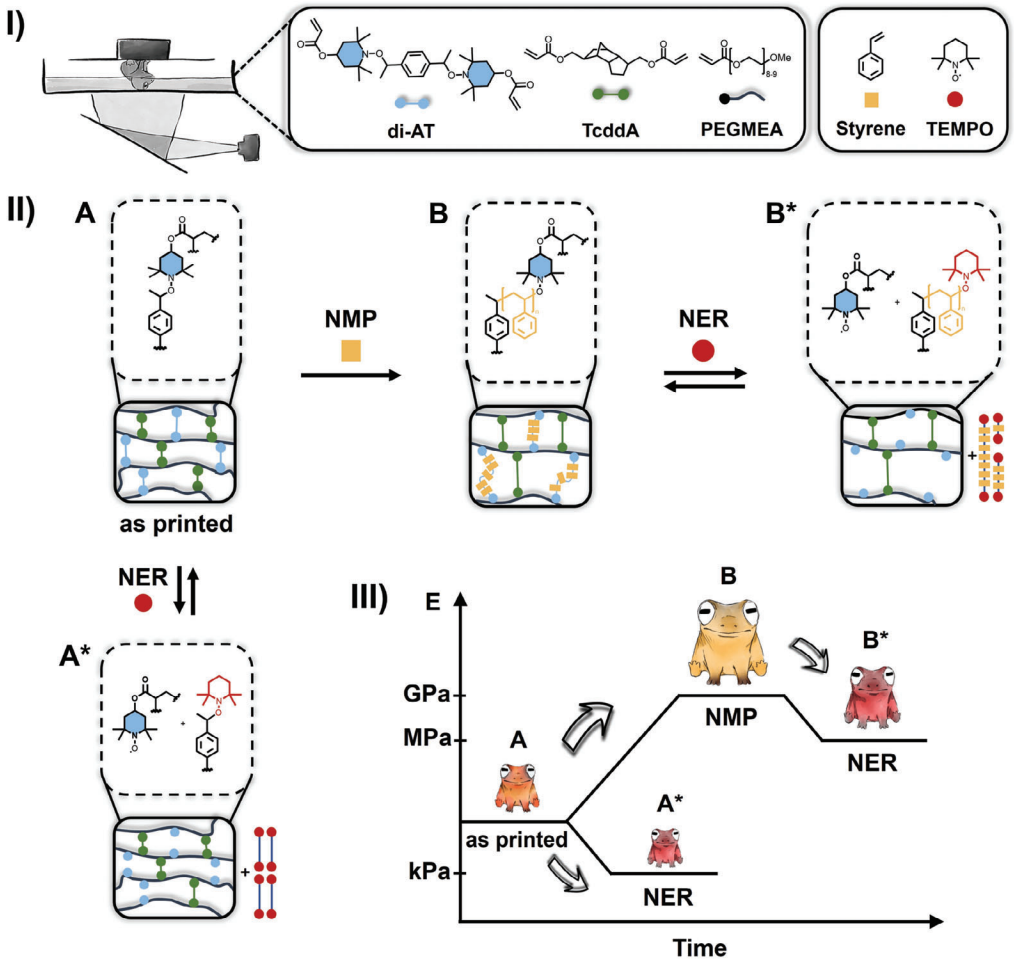

Figure 1. 4D printing of adaptable "living" structures. I) Schematic representation of the DLP printing process and ink formulation based on photo-cross-linkable alkoxyamine species; II) "Multi-way" modification of printed structures A) via nitroxide-mediated polymerization (NMP, B) and nitroxide exchange reaction (NER, A* & B*). III) Schematic representation of the changes in size and mechanical properties of the 4D structures.

well as in mechanical properties (two orders of magnitude for the reduced Young's Modulus). However, the presence of radical quenchers, i.e, TEMPO, in the formulation, limited the amount of functional groups incorporated in the 3D printed network, and therefore functionality. Additionally, the effect was just "one way" and restricted to the microscale regime.

Herein, we introduce an approach that enables the formation of 4D "multi-way" adaptive systems. To achieve this, we designed a multi-functional cross-linker containing two dynamic alkoxyamine and two acrylate functionalities to enable the incorporation of a high degree of functional groups in the printed network without hindering the printing process (**Figure 1**I). Furthermore, the absence of free nitroxide radicals in the formulations will circumvent previous limitations. Digital light processing (DLP) was selected as the 3D printing technique, giving access to complex objects while allowing high resolution. Making use of the dynamic and living characteristics of the alkoxyamine bond, the 3D printed structures were modified by NMP using styrene for the network extension, as well as by NER for network softening, in different sequences (Figure 1II). As a result, the "living" printed structures can undergo both "growth" by chain extension and "degrowth" by nitroxide exchange, where the reduced Young's Modulus can be adapted over a large range (from 770 kPa to 1.2 GPa) (Figure 1III).

2. Results and Discussion

2.1. Design of the "Living" Ink System for DLP Printing

With the aim of 3D printing structures that exhibit "life-like" behavior by undergoing both "growth" and "degrowth" as well as by adapting their mechanical properties, the design of a suitable "living" ink was the first step. A cross-linker di-AT containing alkoxyamines to enable these features was synthesized. In particular, a multi-functional cross-linker equipped with two alkoxyamine and two acrylate groups was designed. Information about the synthesis procedure of di-AT is provided in the Supporting Information (see Scheme S1, Supporting Information). The desired product was obtained as a colorless crystalline solid and carefully characterized by NMR spectroscopy (see Figures S1–S5, Supporting Information).

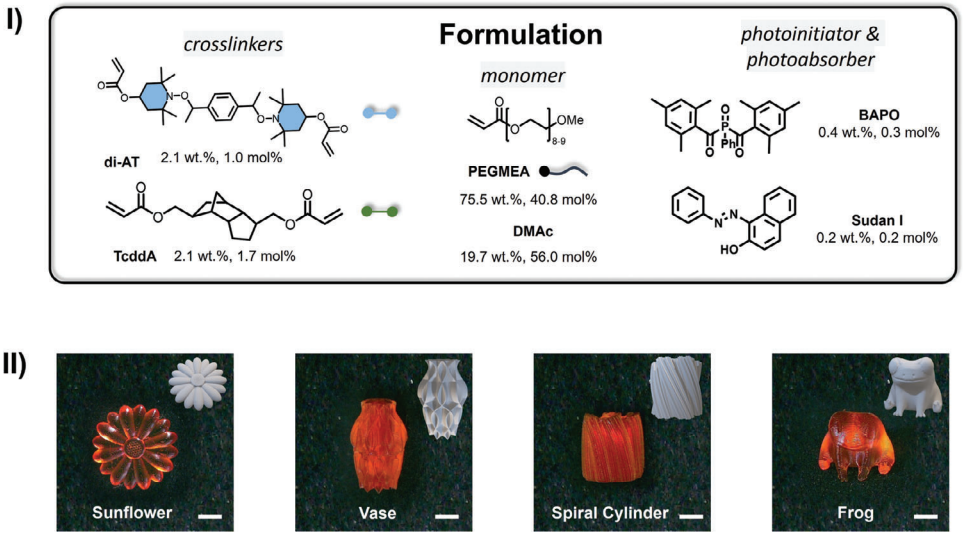

Figure 2. I) Composition of the "living" ink system; II) 3D printed structures (orange) and models (grey): sunflower, vase, spiral cylinder, and frog (from left to right). Scalebar: 2 mm.

In the next step, the synthesized cross-linker was formulated into a corresponding ink suitable for DLP 3D printing. To this end, additional monomers as well as a suitable photoinitiator and other additives are necessary to ensure good printability. In this case, a monofunctional poly(ethylene glycol) methyl ether acrylate (PEGMEA, Mn = 480 g mol^{-1}) was selected as the main monomer. This soft monomer acts as a reactive diluent providing flexibility to the created network facilitating the targeted modifications and adaptivity (see next section). Besides our functional cross-linker di-AT, an additional cross-linker, i.e., tricyclo[5.2.1.0^{2,6}]decanedimethanol diacrylate (TcddA) was added to ensure mechanical integrity of the printed structure by increasing the amount of covalent cross-links. Phenylbis(2,4,6-trimethyl-benzoyl) phosphine oxide (BAPO) was chosen as a suitable radical photoinitiator at the wavelength of employed DLP 3D printing system (385 nm) and Sudan I was selected as a photoabsorber to increase resolution. To ensure homogeneity, especially due to the limited solubility of di-AT in the monomer mixture, the solvent dimethyl acetamide was added to the formulation. Thus, the optimized formulation is composed of PEGMEA (1, 75.5 wt%, 40.8 mol%), the cross-linkers TcddA (2, 2.1 wt%, 1.7 mol%) and di-AT (3, 2.1 wt%, 1.0 mol%), BAPO (4, 0.4 wt%, 0.3 mol%) as photoinitiator and Sudan I (5, 0.2 wt%, 0.2 mol%). and dimethyl acetamide (19.7 wt%, 56.0 mol%) as additives (**Figure 2I**).

Optimal printing parameters such as irradiation time and intensity were carefully identified by performance of curing tests utilizing the UV-LED of the DLP 3D printer (see Supporting Information for detailed information). Jacobs working curves based on the Beer-Lambert law were determined at a curing intensity of 21.0 mW cm^{-2}.[53] The critical energy (E_c) value for gelation and the penetration depth (Dp) of the ink were determined to be 60.2 mJ cm^{-2} and 0.09 mm respectively (see Equation S1 and Figure S6, Supporting Information). Based on these results, the curing time per layer was set to 8 s at a fixed curing intensity of 21 mW cm^{-2}, allowing good printability with a layer thickness of 75 µm.

Having set the printing parameters, the performance of the materials in terms of 3D printability was evaluated. For this purpose, a wide range of complex 3D geometries were fabricated displaying more intricate structural features as well as overhangs. For example, 3D architectures resembling a sunflower, a frog as well as a vase and a spiral cylinder were manufactured (see Figure 2II). Underlining the excellent printing properties, remarkable surface quality was achieved – visible by the smooth transition between the individually cured layers.

2.2. Toward 4D "Living" Structures

Once the printing parameters were optimized, alkoxyamine chemistry was exploited for the preparation of "multi-way" adaptive systems. These adaptive features rely on the reversible cleavage of the alkoxyamine groups, generating a persistent nitroxide radical, which can initiate a controlled polymerization (NMP) or exchange with other nitroxide radicals (NER). In this work, both NMP and NER were employed to induce complex changes in both, size as well as mechanical properties, of the 3D-printed structures. For this purpose, samples with a sunflower geometry (4.50 × 4.50 × 2.00 mm^3) were printed and tested. The modification of the sunflowers was monitored by Fourier transform infrared (FTIR) spectroscopy. Furthermore, electron paramagnetic resonance (EPR) spectroscopy was performed to observe generated radical active species. The changes in the mechanical properties were carefully characterized by nanoindentation. In particular, reduced Young's modulus and hardness were evaluated.

2.2.1. "Growing" by NMP Chain Extension

Styrene was chosen as a suitable monomer for the chain extension, as it can be easily polymerized by NMP, generating a rigid and stiff polymer that exhibits a glass transition temperature at 100 °C.[54,55] Thus, a change in both size (growth) and stiffness

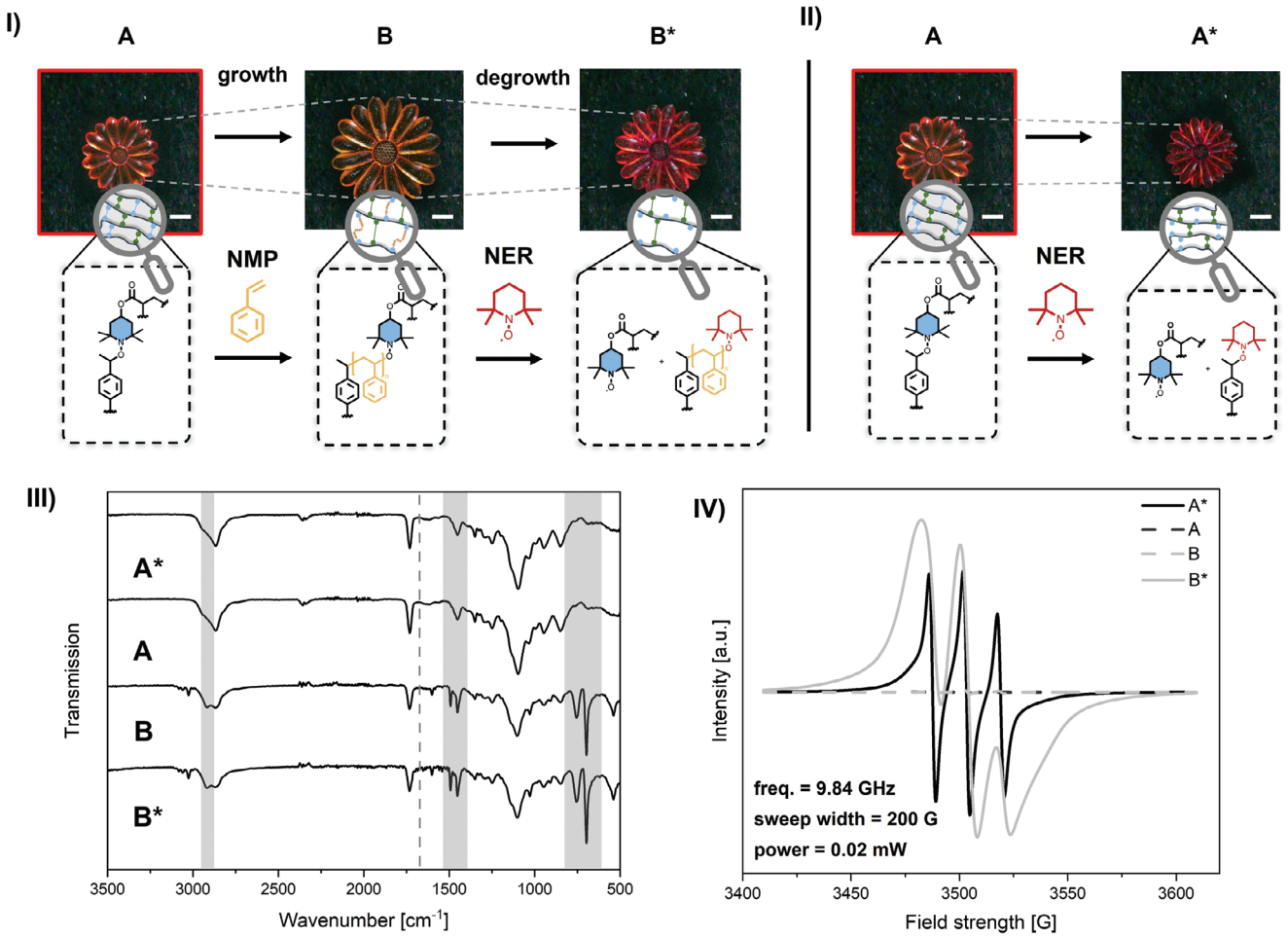

Figure 3. I) Photographs of the sunflower structures as well as the schematic representation of the network change at different stages. A: printed structure, B: NMP modified printed structure, B*: NER modified from B; II) A: printed structure, A*: NER modified printed structure; III) FTIR spectra of samples A, A*, B, B*; IV) EPR spectra of the samples A, A*, B, B*. Scalebar: 2 mm.

(from soft to stiff) was expected (A → B), enabling facile evaluation of successful modification of the material.

Besides the selection of reaction temperature and monomer, another important consideration was diffusion of the monomer inside the printed network to ensure homogeneity. Thus, the 3D-printed sunflowers (A) were immersed overnight in styrene, ensuring sufficient monomer diffusion. Subsequently, NMP polymerization was carried out at 125°C while gently stirring to further improve diffusion of the monomer into the network during the polymerization. FTIR spectroscopy was employed to monitor the progress of the reaction, where spectra of the modified 3D structures were recorded at different reaction times (see Figures S7 and S8, Supporting Information). Within the first hour, polystyrene-specific signals including the aromatic C-C stretching bands at 1450, 1492, and 1601 cm^{-1} as well as the out-of-plane deformation bands of the backbone at 699 and 758 cm^{-1} arose. In addition, the intensity of the distinctive aromatic signals between 1700 and 2000 cm^{-1} increased with ongoing reaction progress, indicating incorporation of styrene in the network, while the absorption band at 1732 cm^{-1} corresponding to the carbonyl stretching band of the PEGMEA network decreased over the reaction progress (**Figure 3**III; see Figure S11, Supporting Information). Importantly, the spectra were measured on the surface of modified structures as well as at the cross-section –, i.e., inside the bulk – and both appeared identical, demonstrating homogenous modification throughout the whole 3D printed structure. Also, a clear change in appearance of the sunflowers was observed. They visually increased in size and also exhibited an increase in stiffness due to incorporation of polystyrene chains. Additionally, a noticeable color shift from orange to white/yellow was observed, serving as an additional indicator of the increased polystyrene content. It is crucial to acknowledge that factors such as the decrease in Sudan I concentration within the structures due to leakage during swelling, along with the increase in structural dimensions during NMP growth, might contribute to the observed color change. To further characterize the effect of incorporating polystyrene, nanoindentation measurements were carried out to determine the changes in the mechanical properties. Cubic samples (2 × 2 × 0.5 mm^3) were printed, chain extended using the same conditions as above and compared with the initial state. The cubic geometry was selected in this case to ensure a flat surface for the nanoindentation measurements. The

as-printed structure (A) exhibited a reduced Young's modulus of 4.3 ± 1.0 MPa and a value for hardness of 0.8 ± 0.5 MPa. After chain extension with styrene, the structures (B) showed a dramatic increase in both properties. In particular the reduced Young's modulus rose by three orders of magnitude to a value of 1182.4 ± 165.0 MPa and a value for hardness of 69.0 ± 24.6 MPa, proving once again the successful chain extension.

2.2.2. "Degrowing" and Softening by NER

As stated above, the incorporated alkoxyamine bond also provides a mechanism for dynamic bond "disconnection" by reversible homolysis of alkoxyamines in the presence of an excess of (2,2,6,6-tetramethylpiperidin-1-yl)oxyl (TEMPO) via the NER reaction pathway. It is expected that the changes generated in the polymer network of the printed structures due to this exchange reaction have an impact on their properties allowing for further additional features.

First, we made use of the nitroxide exchange reaction (NER) to induce "degrow" of the 3D printed sunflower-like structures by cleaving the previously inserted polystyrene chains adding an excess of TEMPO (B → B*, Figure 3I).Due to the bifunctionality of the employed dialkoxyamine both polystyrene "ends" can react with TEMPO, resulting in the removal of linear chains and consequently, in a decrease of the size and stiffness. Furthermore, a color change from orange (B) toward more intense red (B*), due to the generation of stable nitroxide species within the network was observed.[56] Further support is provided by EPR characterization showing clear paramagnetic behavior, in contrast to the EPR silent initial B state, exhibiting diamagnetic features (see Figure 3IV; Figure S12, Supporting Information). Additionally, the cleaved material was analyzed by NMR spectroscopy revealing the presence of the expected polystyrene chains (see Figure S5, Supporting Information) and further proving the mechanism. All NMR signals are in agreement with reference spectra of polystyrene.[39] The effect in the mechanical properties was investigated once again by nanoindentation of cubic samples after NER (B*), which exhibited a reduced modulus of 740.3 ± 65.2 MPa and a hardness of 32.6 ± 7.7 MPa (see Figure S13, Supporting Information). By comparing with the previous data, the value is intermediate between A and B, indicating that only partial cleavage of polystyrene chains occurred. This observation is also in agreement with the volume changes of the sunflowers, whose size was also intermediate between Stage A and B.

Second, NER was also carried out on the "as printed" structures by the addition of TEMPO (A → A*). In this case, a reduction of the cross-linking density was expected due to a decrease of covalent bonds in the alkoxyamine-containing network. Indeed, a slight decrease in size, along with a color change toward red as well as softening of the sunflowers was observed (Figure 3II). To gain more insights into the effect, the modified samples were carefully analyzed by different techniques. Although no clear changes were observed by FTIR spectroscopy, characterization by EPR revealed a distinct signal with a resulting g-value of 2.006, similar to reported values in nitroxide reference spectra[57] and characteristic for TEMPO radical moieties remaining in the network indicating successful NER modification (see Figure 3II). It should be noted that the shape of the signal obtained for stage

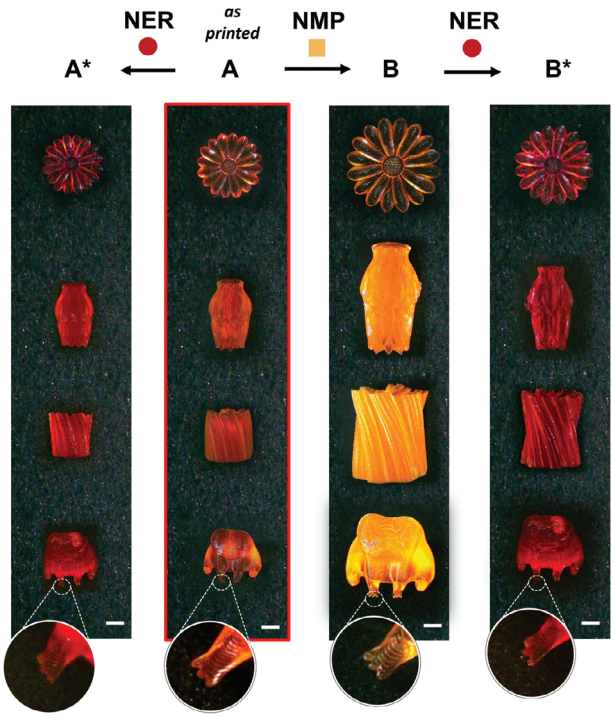

Figure 4. 4D "living" complex structures. Photographs of sunflowers, vases, spiral cylinders, and frogs (from top to down): A* = NER modified; A = as-printed; B = NMP modified using styrene and B* = NER modified from B. Scalebar: 2 mm.

B* is slightly different. This might be the effect of remaining polystyrene chains as NER modification was only partially completed. Consequently, a large variety in the immediate environment of the radical species exists. In addition, nanoindentation measurements were carried out and the NER-modified sample (A*) exhibited, as expected, a lower reduced Young's Modulus as well as hardness. A reduced modulus in the range of 770 kPa–3.6 MPa and a hardness in the range of 20–860 kPa was measured, supporting effects of NER-associated cross-linking density decrease.

2.3. 4D Complex Geometries

In the final step, we expanded the developed approach to more complex geometries. Here we focus in particular on the maintenance of the structural quality during modification. For this purpose, we employed the designed reaction protocols for NMP with styrene as well as NER and applied these to a library of 3D geometries (see **Figure 4**). It should be highlighted that great structural quality was maintained for all three accessible states including A* (direct NER on as-printed stage A), B ("grown" stage), and B* ("degrown" stage). Exemplary of the high level of geometrical preservation is the excellent maintenance of fine features such as the inner part of the flower, the surface patterns of the vase and spiral cylinder as well as the frogs' fingers. As before, the slight reduction in volume as well as the intense red color proved the success of the NER (Figure 4A*).

3. Conclusion

In summary, this work has successfully demonstrated the use of alkoxyamine chemistry as a potential tool for the creation of 4D complex adaptive systems. First, we designed a functional ink for DLP 3D printing. A key component for the implementation of such "living" features was the dialkoxyamine cross-linker di-AT giving access to excellent 3D printability features while avoiding previously reported issues due to radical inhibition. In addition to the high quality of the 3D printed architectures, the application of developed NER and NMP procedures offered "multi-way" adaptability. In particular, the printed structures underwent both "growth" and "degrowth", as well as changes in their mechanical properties. While covering a property window from kPa to GPa for reduced Young's moduli – more than 3 orders of magnitude – excellent structural preservation was achieved for all modified geometries. We believe our approach is a versatile platform that can be easily fine-tuned in the near future by the inclusion of other functional alkoxyamines and monomers and we envision great opportunities especially in fields such as soft robotics, fluidics, or engineering in general where precisely fabricated and adaptable 3D geometries are highly desired.

4. Experimental Section

Materials and Characterization: Tricyclo[5.2.1.0^{2,6}]decanedimethanol diacrylate (TcddA), phenylbis(2,4,6-trimethyl-benzoyl)phosphine oxide (97%, BAPO), Sudan I (Dye content ≥95%), poly(ethylene glycol) methyl ether acrylate (average Mn = 480 g mol^{-1}, contains 100 ppm of BHT as inhibitor, PEGMEA), hydrobromic acid (48%, HBr), triethylamine (99.5%, NEt_3), phenylhydrazine (97%), acryloyl chloride (contains 400 ppm phenolthiazine as stabilizer), N,N,N',N'',N''-pentamethyl-diethylenetriamine (99%) and silica gel (technical grade, pore size 60 Å) were purchased from Sigma–Aldrich. Styrene (99%) was obtained from Merck. Dimethylacetamide (99%) was purchased from VWR. 2,2,6,6-tetramethylpiperidine-1-oxyl (98%, TEMPO) and copper(I) bromide (98%, CuBr) were purchased from Fisher Scientific. Solvents were purchased from Sigma–Aldrich GmbH, Fisher Scientific and Merck, or the Heidelberg University Chem-Store. Reagents were used without further purification, if not mentioned otherwise. Anhydrous solvents were dispensed from a Solvent Purification System MB SPS-800.

Ink Formulation: First, the solid components – Sudan I (7.5 mg, 0.2 wt%), TcddA (75 mg, 2.1 wt%), BAPO (15 mg, 0.4 wt%), and di-AT (75 mg, 2.1 wt%) were- weighted and placed into a brown vial. Afterward, the liquid monomer PEGMEA (2700 mg, 75.5 wt%) and the solvent DMAc (700 mg, 19.7 wt%) were added. To ensure complete solution, the inks were sonicated at 40–50 °C for 30 min and stored in dark.

DLP 3D Printing: DLP 3D printing was performed with an Asiga MAX X27 DLP printer with a 27 µm pixel resolution. A hand-made aluminum build platform with a surface size of 25 × 25 mm^2 was used. An aluminum inlet was added to the commercial ink tray and secured in position using Sylgard 184 silicone elastomer, which was cured at room temperature for 48 h. The Composer software (Asiga, Australia) was used to slice the STL files of all printed structures with the specified z-layer thickness of 50–75 µm before uploading them to the 3D printer. The 3D printing was carried out in at rt in a yellow-light laboratory The fabricated structures were developed in acetone for 1 h and stored in the same solvent until further usage.

"Growth": NMP chain extension was conducted by placing the printed structures in a 50 mL round bottom flask containing a stirring bar. Subsequently, the structures were immersed with 5 to 10 mL of styrene. The mixture was allowed to degas for an hour by nitrogen bubbling. The reaction was gently stirred (100 rpm) for 1 to 4 h at 125 °C. After cooling, the modified structures were carefully washed in THF and ethanol, and dried under vacuum- at rt overnight.

"Degrowth": NER modification was performed by placing the printed structures in a 100 mL round bottom flask with a solution containing an excess of 2,2,6,6-tetramethylpiperidine-1-oxyl (TEMPO) (1.4 g) dissolved in toluene (40 mL) and methanol (10 mL). The mixture was degassed for 1 h and subsequently stirred at 100 °C for 8 h under a nitrogen atmosphere. The samples were then filtered and washed using THF and methanol to remove unreacted TEMPO. The resulting structures were vacuum-dried at rt overnight. The filtrate was vacuum-dried and precipitated using methanol.

EPR Measurements: EPR measurements were carried out using a Bruker EMXmicro-6/1/P/L (SN: EMM 2311) system with an ER 070 magnet. Software from Bruker called Xenon was used to examine the resulting spectra.

Fourier Transformation Infrared Spectroscopy (FT-IR): A Jasco FT/IR-4600 spectrometer was used to measure FTIR spectra under ambient conditions. 16 scans were recorded at a bandwidth of 500 to 4000 cm^{-1} for each sample. All samples were thoroughly dried prior to measurements.

Nanoindentation Measurements: Nanoindentation measurements were performed on a Bruker Hysitron TI 980 Nanoindenter equipped with a low-load head and using a diamond Berkovich tip. Before the measurements, the indentation tip was calibrated against air and the tip area function was calculated. The measurements were performed at room temperature in displacement-controlled mode applying a trapezoid loading function with a loading and unloading rate of 200 nm s^{-1}, a peak displacement of 1000 nm, and automatic drift control. For all samples, n = 5 measurements were performed, and a mean value and standard deviation was calculated. The reduced modulus and the hardness values were determined according to literature, from the slope of the tangent of the elastic unloading curve from the load–displacement curve and represents the elastic deformation in the microstructures.[58] Note: for A* a displacement-controlled, multiple partial unloading approach was used, taking n = 5 representative curves.

Supporting Information

Supporting Information is available from the Wiley Online Library or from the author.

Acknowledgements

E.B. acknowledges the funding from the Excellence Cluster "3D Matter Made to Order" (EXC-2082-390761711) and the Carl Zeiss Foundation through the "Carl-Zeiss-Foundation-Focus@HEIKA". E.B. also acknowledges funding by the SPP 2206 – DFG Priority program "Cooperative Multistage Multistable Microactuator Systems". (BL1604/5-2) The authors thank Luna Garcia (Universidad Autónoma de Barcelona) for helpful support regarding the DLP printer and Dr. Markus Kurth for help regarding EPR measurements. The authors thank Dr. Maximillian Hackner for support with nanoindentation measurements.

Conflict of Interest

The authors declare no conflict of interest.

Data Availability Statement

The data that support the findings of this study are available from the corresponding author upon reasonable request.

Keywords

covalent adaptable networks, digital light processing, life-like materials, nitroxides, photopolymerization

Received: November 30, 2023
Revised: January 5, 2024
Published online: January 18, 2024

[1] S. C. Ligon, R. Liska, J. Stampfl, M. Gurr, R. Mülhaupt, *Chem. Rev.* **2017**, *117*, 10212.
[2] J. R. Tumbleston, D. Shirvanyants, N. Ermoshkin, R. Janusziewicz, A. R. Johnson, D. Kelly, K. Chen, R. Pinschmidt, J. P. Rolland, A. Ermoshkin, E. T. Samulski, J. M. Desimone, *Science* **2015**, *347*, 1349.
[3] L. A. E. Müller, A. Demongeot, J. Vaucher, Y. Leterrier, J. Avaro, M. Liebi, A. Neels, I. Burgert, T. Zimmermann, G. Nyström, G. Siqueira, *ACS Appl. Mater. Interfaces* **2022**, *14*, 16703.
[4] Y. Zhang, Z. Dong, C. Li, H. Du, N. X. Fang, L. Wu, Y. Song, *Nat. Commun.* **2020**, *11*, 4685.
[5] M. A. Skylar-Scott, J. Mueller, C. W. Visser, J. A. Lewis, *Nature* **2019**, *575*, 330.
[6] D. A. Walker, J. L. Hedrick, C. A. Mirkin, *Science* **2019**, *366*, 360.
[7] Y. Chao, Q. Chen, Z. Liu, *Adv. Funct. Mater.* **2020**, *30*, 1902785.
[8] R. D. Field, P. N. Anandakumaran, S. K. Sia, *Appl. Phys. Rev.* **2019**, *6*, 041305.
[9] G. Palmara, F. Frascella, I. Roppolo, A. Chiappone, A. Chiadò, *Biosens. Bioelectron.* **2021**, *175*, 112849.
[10] C. Chen, B. T. Mehl, A. S. Munshi, A. D. Townsend, D. M. Spence, R. S. Martin, *Anal. Methods* **2016**, *8*, 6005.
[11] S. Waheed, J. M. Cabot, N. P. Macdonald, T. Lewis, R. M. Guijt, B. Paull, M. C. Breadmore, *Lab Chip* **2016**, *16*, 1993.
[12] N. Weigel, M. J. Männel, J. Thiele, *ACS Appl. Mater. Interfaces* **2021**, *13*, 31086.
[13] S. Nocentini, C. Parmeggiani, D. Martella, D. S. Wiersma, *Adv. Opt. Mater.* **2018**, *6*, 1800207.
[14] J. Shintake, V. Cacucciolo, D. Floreano, H. Shea, *Adv. Mater.* **2018**, *30*, 1707035.
[15] M. Medina-Sánchez, V. Magdanz, M. Guix, V. M. Fomin, O. G. Schmidt, *Adv. Funct. Mater.* **2018**, *28*, 1707228.
[16] M. Champeau, D. A. Heinze, T. N. Viana, E. R. De Souza, A. C. Chinellato, S. Titotto, *Adv. Funct. Mater.* **2020**, *30*, 1910606.
[17] M. Hippler, E. Blasco, J. Qu, M. Tanaka, C. Barner-Kowollik, M. Wegener, M. Bastmeyer, *Nat. Commun.* **2019**, *10*, 232.
[18] J.-Y. Wang, F. Jin, X.-Z. Dong, J. Liu, M.-L. Zheng, *Adv. Mater. Technol.* **2022**, *7*, 2200276.
[19] M. Gou, X. Qu, W. Zhu, M. Xiang, J. Yang, K. Zhang, Y. Wei, S. Chen, *Nat. Commun.* **2014**, *5*, 3774.
[20] M. Caprioli, I. Roppolo, A. Chiappone, L. Larush, C. F. Pirri, S. Magdassi, *Nat. Commun.* **2021**, *12*, 2462.
[21] J. Torgersen, X.-H. Qin, Z. Li, A. Ovsianikov, R. Liska, J. Stampfl, *Adv. Funct. Mater.* **2013**, *23*, 4542.
[22] H. Zeng, P. Wasylczyk, C. Parmeggiani, D. Martella, M. Burresi, D. S. Wiersma, *Adv. Mater.* **2015**, *27*, 3883.
[23] A. Münchinger, V. Hahn, D. Beutel, S. Woska, J. Monti, C. Rockstuhl, E. Blasco, M. Wegener, *Adv. Mater. Technol.* **2022**, *7*, 2100944.
[24] M. Gastaldi, C. A. Spiegel, C. Vazquez-Martel, C. Barolo, I. Roppolo, E. Blasco, *Mol. Syst. Des. Eng.* **2023**, *8*, 323.
[25] C. A. Spiegel, M. Hackner, V. P. Bothe, J. P. Spatz, E. Blasco, *Adv. Funct. Mater.* **2022**, *32*, 2110580.
[26] W. Zhang, H. Wang, H. Wang, J. Y. E. Chan, H. Liu, B. Zhang, Y.-F. Zhang, K. Agarwal, X. Yang, A. S. Ranganath, H. Y. Low, Q. Ge, J. K. W. Yang, *Nat. Commun.* **2021**, *12*, 112.
[27] M. P. Jeske, W. Zhang, M. Anthamatten, *Adv. Mater. Technol.* **2022**, *7*, 2101725.
[28] A. Bagheri, K. E. Engel, C. W. A. Bainbridge, J. Xu, C. Boyer, J. Jin, *Polym. Chem.* **2020**, *11*, 641.
[29] M. Asadi-Eydivand, T. C. Brown, A. Bagheri, *ACS Appl. Polym. Mater.* **2022**, *4*, 4940.
[30] A. Bagheri, H. Ling, C. W. A. Bainbridge, J. Jin, *ACS Appl. Polym. Mater.* **2021**, *3*, 2921.
[31] A. Bagheri, *Macromolecules* **2023**, *56*, 1778.
[32] G. Zhu, H. A. Houck, C. A. Spiegel, C. Selhuber-Unkel, Y. Hou, E. Blasco, *Adv. Funct. Mater.* 2300456.
[33] C. J. Kloxin, T. F. Scott, B. J. Adzima, C. N. Bowman, *Macromolecules* **2010**, *43*, 2643.
[34] J. J. Hernandez, A. L. Dobson, B. J. Carberry, A. S. Kuenstler, P. K. Shah, K. S. Anseth, T. J. White, C. N. Bowman, *Macromolecules* **2022**, *55*, 1376.
[35] M. Podgórski, S. Huang, C. N. Bowman, *ACS Appl. Mater. Interfaces* **2021**, *13*, 12789.
[36] C. J. Kloxin, C. N. Bowman, *Chem. Soc. Rev.* **2013**, *42*, 7161.
[37] M. Podgórski, B. D. Fairbanks, B. E. Kirkpatrick, M. Mcbride, A. Martinez, A. Dobson, N. J. Bongiardina, C. N. Bowman, *Adv. Mater.* **2020**, *32*, 1906876.
[38] Y. Amamoto, H. Otsuka, A. Takahara, K. Matyjaszewski, *Adv. Mater.* **2012**, *24*, 3975.
[39] Y. Jia, Y. Matt, Q. An, I. Wessely, H. Mutlu, P. Theato, S. Bräse, A. Llevot, M. Tsotsalas, *Polym. Chem.* **2020**, *11*, 2502.
[40] J. J. Cash, T. Kubo, A. P. Bapat, B. S. Sumerlin, *Macromolecules* **2015**, *48*, 2098.
[41] N. Zheng, Y. Xu, Q. Zhao, T. Xie, *Chem. Rev.* **2021**, *121*, 1716.
[42] Q. An, I. D. Wessely, Y. Matt, Z. Hassan, S. Bräse, M. Tsotsalas, *Polym. Chem.* **2019**, *10*, 672.
[43] C. N. Bowman, C. J. Kloxin, *Angew. Chem., Int. Ed.* **2012**, *51*, 4272.
[44] Y. Jia, G. Delaittre, M. Tsotsalas, *Macromol. Mater. Eng.* **2022**, *307*, 2200178.
[45] K. Jin, L. Li, J. M. Torkelson, *Adv. Mater.* **2016**, *28*, 6746.
[46] G. Audran, P. Brémond, S. R. A. Marque, *Chem. Commun.* **2014**, *50*, 7921.
[47] H. Otsuka, *Polym. J.* **2013**, *45*, 879.
[48] B. Schulte, M. Tsotsalas, M. Becker, A. Studer, L. De Cola, *Angew. Chem., Int. Ed.* **2010**, *49*, 6881.
[49] I. Wessely, V. Mugnaini, A. Bihlmeier, G. Jeschke, S. Bräse, M. Tsotsalas, *RSC Adv.* **2016**, *6*, 55715.
[50] I. D. Wessely, Y. Matt, Q. An, S. Bräse, M. Tsotsalas, *RSC Adv.* **2021**, *11*, 27714.
[51] M. Belqat, X. Wu, J. Morris, K. Mougin, T. Petithory, L. Pieuchot, Y. Guillaneuf, D. Gigmes, J.-L. Clément, A. Spangenberg, *Adv. Funct. Mater.* **2023**, *33*, 2211971.
[52] Y. Jia, C. A. Spiegel, A. Welle, S. Heißler, E. Sedghamiz, M. Liu, W. Wenzel, M. Hackner, J. P. Spatz, M. Tsotsalas, E. Blasco, *Adv. Funct. Mater.* **2023**, *33*, 2207826.
[53] P. F. Jacobs, *Rapid Prototyping & Manufacturing: Fundamentals of Stereolithography*, Society of Manufacturing Engineers, Dearborn, MI **1992**.
[54] J. Rieger, *J. Therm. Anal. Calorim.* **2005**, *46*, 965.
[55] C. J. Hawker, In *Handbook of Radical Polymerization*, Wiley, Hoboken, NJ, USA **2002**, p. 463.
[56] A. W. Hui, A. E. Hamielec, *J. Appl. Polym. Sci.* **1972**, *16*, 749.
[57] A. I. Smirnov, T. I. Smirnova, P. D. Morse, *Biophys. J.* **1995**, *68*, 2350.
[58] W. C. Oliver, G. M. Pharr, *J. Mater. Res.* **1992**, *7*, 1564.